Available online at www.sciencedirect.com
ScienceDirect
International Journal of Heat and Mass Transfer 49 (2006) 4932–4942
International Journal of HEAT and MASS TRANSFER
www.elsevier.com/locate/ijhmt

Buoyancy and wall conduction effects on forced convection of micropolar fluid flow along a vertical slender hollow circular cylinder

Cheng-Long Chang

Department of Mechanical Engineering, Hsiuping Institute of Technology, Dali, Taichung 41280, Taiwan, ROC

Received 2 November 2005; received in revised form 24 April 2006
Available online 17 August 2006

Abstract

This paper presents a numerical analysis of the flow and heat transfer characteristics of forced convection in a micropolar fluid flowing along a vertical slender hollow circular cylinder with wall conduction and buoyancy effects. The non-linear formulation governing equations and their associated boundary conditions are solved using the cubic spline collocation method and the finite difference scheme with a local non-similar transformation. This study investigates the effects of the conjugate heat transfer parameter, the Richardson number, the micropolar parameter, and the Prandtl number on the flow and the thermal fields. The effect of wall conduction on the thermal and the flow fields are found to be more pronounced in a system with a greater buoyancy effect or Prandtl number but is less sensitive with a greater micropolar material parameter. Compared to the case of pure forced convection, buoyancy effect is found to result in a lower interfacial temperature but higher the local heat transfer rate and the skin friction factor. Finally, compared to Newtonian fluid, an increase in the interfacial temperature, a reduction in the skin friction factor, and a reduction in the local heat transfer rate are identified in the current micropolar fluid case.

Keywords: Conjugate heat transfer parameter; Buoyancy effect; Micropolar fluid; Slender cylinder

1. Introduction

Buoyancy effects become fundamentally important in forced convection when the fluid velocity is relatively low or when the temperature difference between the wall and the free stream is large. Under these conditions, the density gradient generated by the temperature difference responsible for the buoyancy convection effects must be taken into consideration. It is also important to analyze the case of mixed convection, when the order of magnitude of the forced convection and the free convection are equal. Many practical applications of mixed convection exist, including in the fuel element of a nuclear reactor, in the heaters and coolers of mechanical or chemical devices, in the lubrication of machine parts, etc.

The influence of thermal buoyancy effects on forced convection has been studied extensively by many investigators. Lloyd and Sparrow [1] used a local similarity method to solve the mixed convection flow on a vertical surface and showed that the numerical solutions ranged from pure forced convection to mixed convection. Chen and Mucoglu [2] analyzed the buoyancy and transverse curvature effects on forced convection of Newtonian fluid flow along an isothermal vertical cylinder using the local non-similarity method. The same problem for a uniform surface heat flux case was conducted by Mucoglu and Chen [3]. The effect of air property variations in the boundary layer flow along a moving cylinder was investigated by Choi [4]. Lee et al. [5] studied the problem of mixed convection along a vertical cylinder with uniform surface heat flux for the entire mixed convection regime, ranging from pure forced convection to pure free convection by employing the buoyancy and curvature parameters. The unsteady forced convection

E-mail address: clchang@mail.hit.edu.tw

0017-9310/$ - see front matter © 2006 Elsevier Ltd. All rights reserved.
doi:10.1016/j.ijheatmasstransfer.2006.05.037

Nomenclature

B	dimensionless parameter of microinertia density
C_f	skin friction coefficient
F	reduced stream function
g	gravitational acceleration
G	dimensionless microrotation
Gr	Grashof number
j	microinertia density
K	thermal conductivity
L	length of the cylinder
N	angular velocity of micropolar fluid
Nu_x	local Nusselt number
p	conjugate heat transfer parameter
Pr	Prandtl number
r	coordinate in the radius direction
r_i, r_o	inner and outer radii of the hollow cylinder
Re	Reynolds number
Re_x	local Reynolds number
Ri	Richardson number
T	temperature
T_0	temperature of the inside surface of the cylinder
u, v	velocity components in x and r directions, respectively
x	coordinate along the axis

Greek symbols

α	thermal diffusivity
β	thermal expansion coefficient
γ	spin-gradient viscosity
Δ	dimensionless parameter of vortex viscosity
ζ	dimensionless streamwise coordinate
η	pseudo-similarity variable
θ	dimensionless temperature
κ	vortex viscosity
λ	dimensionless parameter of spin-gradient viscosity
μ	dynamic viscosity
ν	kinematic viscosity
ξ	dimensionless streamwise coordinate
ρ	density of micropolar fluid
σ	transverse curvature parameter
τ	shear stress
φ	stream function

Superscripts

n	false time level of n
$n+1$	false time level of $n+1$
$'$	derivate with respect to η

Subscripts

f	condition in the fluid
s	condition in the wall of cylinder
w	condition at solid–liquid interface
∞	condition in surrounding medium

laminar boundary layer flow over a longitudinal cylinder has been investigated by Eswara and Nath [6]. Their experimental results were found to be consistent with the numerical results of Lloyd and Sparrow [1] and other previous studies.

Recently, Na and Pop [7] considered a thin longitudinal circular cylinder moving in a flowing stream, and obtained the velocity and temperature distributions by using the Keller-box method. The studies of the transient unsteady process of cooling down and stratifying an initially homogeneous fluid by in a vertical circular cylinder were conducted by Lin and Armfield [8]. The effects of localized cooling/heating and injection/suction on the mixed convection flow on a thin vertical cylinder were analyzed by Kumari and Nath [9].

The investigations cited above all considered the fluid to be Newtonian. However, in practice, many of the fluids involved in technical processes and engineering applications exhibit non-Newtonian behavior. Consequently, the analysis of mixed convection must be extended to the case of non-Newtonian fluids. The theory of simple microfluid was originally developed by Eringen [10,11] and has now been applied in the investigation of various fluids. This theory takes the microscopic effects arising from the local structure and micromotions of the fluid elements into account and provides the basis for a mathematical model for non-Newtonian fluids which can be used to analyze the behavior of exotic lubricants, polymers, liquid crystals, animal bloods, and colloidal or suspension solutions, etc. The theory of micropolar fluids has been extensively researched and proved by a number of investigators [12–14]. Lately, Gorla and Ameri [15] studied the mixed convection boundary layer flow on a continuous moving cylinder by using the theory of micropolar fluids formulated by Eringen. Gorla et al. [16] applied the expansion method to conduct the mixed convection heat transfer characteristics of the micropolar fluid flow along an isothermal vertical plate.

More recently, Mohammadien et al. [17] investigated the heat transfer characteristics of the mixed convection flow of micropolar fluids for the case of a moving heated horizontal plate. Siddheshwar and Krishna [18] applied the Fourier series expansion method to conduct the linear and non-linear analyses of convection in a micropolar fluid occupying a porous medium. The mixed convection flow of a continuously moving plate in a moving free stream was investigated by Bhargava et al. [19]. The velocity, microrotation and temperature distribution functions are computed numerically. Meanwhile, in their studies [13–19], the thermal boundary condition at the solid surface was

assumed either prescribed wall temperature or prescribed heat flux, and thus the interaction between the solid surface and its adjacent boundary layer was neglected.

However, in many practical applications, such as heat exchangers, heaters, nuclear reactors, pipe insulation systems, etc., the effect of conduction within the solid wall is significant and must be taken into account. Hence, the analysis of this type of heat transfer mechanisms possesses necessary the coupling of the conduction in the solid body and the convection in the fluid surrounding it. The conjugate heat transfer problem, in which the coupled heat transfer processes between the solid body (conduction mechanisms) and the fluid flow (convection mechanisms) are considered simultaneously, has been investigated by several researchers for the case of a Newtonian fluid.

For example, two-dimensional conjugate heat transfer problems of free convection from a vertical flat plate with a uniform temperature or a uniform heat flux at the outside surface of the plate was studied, numerically and experimentally, by Miyamoto et al. [20]. The conjugate problem for a vertical plate fin with various heat transfer coefficients under forced convection has been investigated by Sparrow and Chyu [21]. They assumed the heat conduction in the fin to be one-dimensional. Timma and Padet [22] employed the extension of Blasius method to investigate the similar problem with a simplification of the axial conduction term in the energy equation of the plate was neglected. Pozzi and Lupo [23] obtained the perturbation solutions for the coupled problem of natural convection along, and conduction within, a heated flat plate. Char et al. [24] employed the cubic spline collocation numerical method to analyze the conjugate heat transfer in the laminar boundary layer on a continuous, moving plate. The effect of wall conduction on the heat transfer characteristics of the natural convection over a vertical slender hollow circular cylinder was investigated by Na [25].

Recently, the conjugate free convection from a slightly inclined flat plate in a porous medium was investigated both analytically and numerically by Vaszi et al. [26]. Finally, Jilani et al. [27] analyzed a heat generating vertical cylinder with two-dimensional heat conduction models and coupled a laminar forced convection flow in the fluid surrounding it. They obtained the numerical solutions by using the finite difference scheme.

In the previous studies, the investigators dealing with conjugate heat transfer problems [20–27] focused on Newtonian fluids flowing along a solid surface. Although the conjugate mixed convection flow of a micropolar fluid along a slender cylinder is of great practical importance in many industrial and theoretical applications, a review of the literature reveals that this problem has yet to be reported. Accordingly, the intention of the present study is to address this perceived lack in the literature. For simplicity, this study assumed the case of a vertical slender hollow cylinder such that the heat conduction within the wall is one-dimensional. The cubic spline collocation method and a finite difference approximation scheme are used to solve the conjugate heat transfer problem. Variation in the fluid–solid interfacial temperature distribution, skin friction factor and the local heat transfer rate are presented to highlight the influence of the wall conduction, buoyancy, and micropolar material parameter. Moreover, the current results are compared with the previous numerical results for the conjugate mixed convection flow of Newtonian fluids along a vertical slender hollow circular cylinder, and are found to be in good agreement.

2. Mathematical formulation

This study considers the case of a micropolar fluid flow past a vertical slender hollow circular cylinder of length L and outer radius r_o ($L \gg r_o$). The physical model and coordinate system are shown in Fig. 1. The gravitational acceleration, g, acts in the downward direction. The temperature and velocity of the micropolar fluid at a distance remote from the cylinder are given by T_∞ and U_∞, respectively. The temperature of the inside surface of the cylinder is maintained at a constant temperature of T_0, where $T_0 > T_\infty$. Other than the density variation, the remaining fluid properties are assumed to be constant. The temperature difference between the body surface and the surrounding micropolar fluid generates a buoyancy force, which results in an upward convective flow. The viscous dissipation is considered to be negligible.

By employing laminar boundary layer flow assumptions and the Boussinesq approximation, the governing equations for the micropolar fluid can be written as

For continuity:

$$\frac{\partial(ru)}{\partial x} + \frac{\partial(rv)}{\partial r} = 0. \tag{1}$$

For momentum:

$$u\frac{\partial u}{\partial x} + v\frac{\partial u}{\partial r} = \left(\nu + \frac{\kappa}{\rho}\right)\frac{1}{r}\frac{\partial}{\partial r}\left(r\frac{\partial u}{\partial r}\right) + \frac{\kappa}{\rho}\left(\frac{N}{r} + \frac{\partial N}{\partial r}\right) + g\beta(T - T_\infty). \tag{2}$$

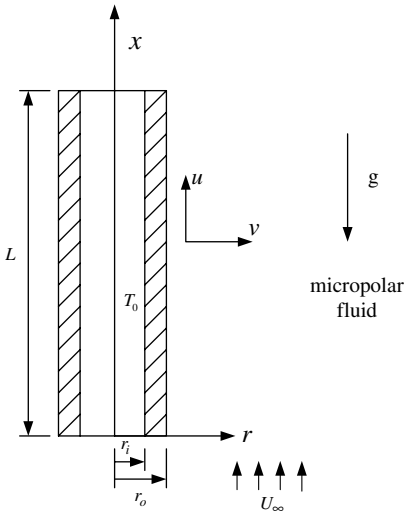

Fig. 1. Physical model and coordinate system.

For angular momentum:

$$u\frac{\partial N}{\partial x}+v\frac{\partial N}{\partial r}=\frac{\gamma}{j\rho}\left[\frac{1}{r}\frac{\partial}{\partial r}\left(r\frac{\partial N}{\partial r}\right)-\frac{N}{r^2}\right]-\frac{\kappa}{j\rho}\left(\frac{\partial u}{\partial r}+2N\right). \tag{3}$$

For energy:

$$u\frac{\partial T}{\partial x}+v\frac{\partial T}{\partial r}=\alpha\frac{1}{r}\frac{\partial}{\partial r}\left(r\frac{\partial T}{\partial r}\right). \tag{4}$$

In the equations above, u and v are the velocity components along the x and r directions, respectively; ρ, ν, α and β are the density, kinematic viscosity, thermal diffusivity and thermal expansion coefficient of the fluid, respectively, and κ, j, and γ are the vortex viscosity, microinertia density, and spin-gradient viscosity of the fluid, respectively. Finally, T is the fluid temperature, and N is the component of microrotation whose direction of rotation lies in the $(x-r)$ plane.

The boundary conditions are given by the following:

$$r=r_0: u=0,\quad v=0,\quad N=-\frac{1}{2}\frac{\partial u}{\partial r},\quad T=T_{\mathrm{w}}(x), \tag{5a}$$

$$r\to\infty: u=U_\infty,\quad N=0,\quad T=T_\infty, \tag{5b}$$

where subscripts w and ∞ refer to the wall and the boundary layer edge, respectively. In addition, $T_{\mathrm{w}}(x)$ is the outer surface temperature of the cylinder, which is not known a priori. The boundary condition given in Eq. (5a) for N at the outer surface of the cylinder, i.e. $r=r_{\mathrm{o}}$, indicates that the microrotation is equal to one half of the fluid vorticity at the boundary (Ahmadi [13] and Jena and Mathur [14]).

One of objective of the current study is to predict the outer surface temperature of the cylinder, $T_{\mathrm{w}}(x)$. Therefore, an additional governing equation is required for the slender hollow cylinder based on the simplification that the wall of cylinder steady transfers its heat to the surrounding micropolar fluid. Since, the outer radius of the hollow cylinder, r_{o}, is small compared to its length, L, the axial conduction term in the heat conduction equation of the cylinder can be omitted [22,23,25]. The governing equation for the temperature distribution within the slender hollow circular cylinder is given by

$$\frac{1}{r}\frac{\partial}{\partial r}\left(r\frac{\partial T_{\mathrm{s}}}{\partial r}\right)=0;\quad 0\leqslant x\leqslant L;\quad r_{\mathrm{i}}<r\leqslant r_{\mathrm{o}}. \tag{6}$$

The boundary conditions for the wall of cylinder are given by

$$\text{At } r=r_{\mathrm{i}},\quad T_{\mathrm{s}}=T_0, \tag{7a}$$

$$\text{At the interface } (r=r_{\mathrm{o}}): T_{\mathrm{s}}=T(x,r_{\mathrm{o}}),\quad -K_{\mathrm{s}}\frac{\partial T_{\mathrm{s}}}{\partial r}=-K_{\mathrm{f}}\frac{\partial T(x,r_{\mathrm{o}})}{\partial r}, \tag{7b}$$

where K_{s} and K_{f} are the thermal conductivity of the cylinder and the fluid, respectively. The boundary conditions given in Eq. (7b) state the physical requirements that the temperature and heat fluxes of the cylinder and the micropolar fluid must be continuous across the solid–fluid interface. From Eqs. (6) and (7b), the temperature distribution T_{w} at the interface is derived as:

$$T_{\mathrm{w}}(x)=T(x,r_{\mathrm{o}})=r_{\mathrm{o}}\frac{K_{\mathrm{f}}}{K_{\mathrm{s}}}\ln\left(\frac{r_{\mathrm{o}}}{r_{\mathrm{i}}}\right)\frac{\partial T(x,r_{\mathrm{o}})}{\partial r}+T_0. \tag{8}$$

To facilitate the solution of this problem, pseudo-similarity variables ζ and η are introduced with the reduced stream function $F(\zeta,\eta)$, the dimensionless microrotation $G(\zeta,\eta)$, and the dimensionless temperature $\theta(\zeta,\eta)$, i.e.

$$\zeta=\tfrac{x}{r_{\mathrm{o}}},\quad \eta=\tfrac{1}{2x}Re_x^{1/2}\left(\tfrac{r^2-r_{\mathrm{o}}^2}{r_{\mathrm{o}}}\right),\quad \varphi=r_{\mathrm{o}}\nu Re_x^{1/2}F(\zeta,\eta),\quad N=\tfrac{r_{\mathrm{o}}U_\infty^2}{\nu r}Re_x^{-1/2}G(\zeta,\eta),\quad \theta=\tfrac{T-T_\infty}{T_0-T_\infty}, \tag{9}$$

where Re_x is the local Reynolds number which is defined as

$$Re_x=\frac{U_\infty x}{\nu}. \tag{10}$$

The stream function, φ, satisfies the continuity equation given in Eq. (1) automatically with

$$u=\frac{1}{r}\frac{\partial\varphi}{\partial r},\quad v=-\frac{1}{r}\frac{\partial\varphi}{\partial x}. \tag{11}$$

Substituting Eq. (9) into the governing momentum, angular momentum, and energy equations, respectively, yields

$$(1+\Delta)[(1+\sigma\eta)F'']'+\frac{1}{2}FF''+\Delta G'+Ri\zeta\theta=\zeta\left(F'\frac{\partial F'}{\partial\zeta}-F''\frac{\partial F}{\partial\zeta}\right), \tag{12}$$

$$\lambda(1+\sigma\eta)G''+\frac{1}{2}FG'+\frac{1}{2}F'G-\frac{\Delta B}{2}\sigma^2G-\frac{1}{4}\left(\frac{\sigma}{1+\sigma\eta}\right)FG+\frac{1}{4}\left(\frac{\sigma}{1+\sigma\eta}\right)\eta F'G-\frac{\Delta B}{4}\sigma^2(1+\sigma\eta)F''=\zeta\left[\frac{1}{2}\left(\frac{\sigma}{1+\sigma\eta}\right)G\frac{\partial F}{\partial\zeta}+F'\frac{\partial G}{\partial\zeta}-G'\frac{\partial F}{\partial\zeta}\right], \tag{13}$$

$$\frac{1}{Pr}(1+\sigma\eta)\theta''+\frac{1}{Pr}\sigma\theta'+\frac{1}{2}F\theta'=\zeta\left(F'\frac{\partial\theta}{\partial\zeta}-\theta'\frac{\partial F}{\partial\zeta}\right). \tag{14}$$

In the equations above, the primes indicate partial differentiation with respect to η alone and $Pr=\nu/\alpha$ is the Prandtl number. Furthermore, the dimensionless parameters Δ, B, and λ characterize the vortex viscosity, the microinertia density, and the spin-gradient viscosity, respectively, and are defined as

$$\Delta=\frac{\kappa}{\rho\nu},\quad B=\frac{r_{\mathrm{o}}^2}{j},\quad \lambda=\frac{\gamma}{j\rho\nu}. \tag{15}$$

In addition, Ri and σ are the Richardson number and transverse curvature parameter, respectively, which are defined as

$$Ri = \frac{Gr}{Re^2}, \quad \sigma = 2\left(\frac{\zeta}{Re}\right)^{1/2}, \tag{16}$$

where Re and Gr are the Reynolds number and Grashof number, respectively, which are defined as

$$Re = \frac{U_\infty r_o}{\nu}, \quad Gr = \frac{g\beta(T_0 - T_\infty)r_o^3}{\nu^2}. \tag{17}$$

Furthermore, Ri is the Richardson number and it is a measure of the relative importance of the buoyancy effect with respect to the forced convection. Therefore, for mixed convection flow, $0 < Ri < \infty$; for pure free convection flow, $U_\infty = 0$, $Re = 0$ and hence $Ri = \infty$; and for pure forced convection flow, the buoyancy is zero, i.e., $Ri = 0$.

Following transformation, the corresponding boundary conditions given in Eqs. (5) and (8) become

At $\eta = 0$:

$$F'(\zeta,0) = 0, \quad F(\zeta,0) = -2\zeta\left.\frac{\partial F}{\partial \zeta}\right|_{\eta=0},$$

$$G(\zeta,0) = -\frac{1}{2}F''(\zeta,0), \quad p\zeta^{-1/2}\theta'(\zeta,0) = \theta(\zeta,0) - 1. \tag{18a}$$

As $\eta \to \infty$:

$$F'(\zeta,\infty) = 1, \quad G(\zeta,\infty) = \theta(\zeta,\infty) = 0, \tag{18b}$$

where $p = \frac{K_f}{K_s}\ln\left(\frac{r_o}{r_i}\right)Re^{1/2}$ is the conjugate heat transfer parameter. It should be noticed that for the limiting case of $p = 0$, the thermal boundary condition in Eq. (18a) on the wall becomes isothermal. Intuitively, if the heat conductivity of the hollow cylinder is very large, its temperature can be expected to be approximately uniform at T_0. Hence, the magnitude of p determines the importance of the wall heat conduction effect.

For Newtonian fluid flow ($\Delta = 0$), Eqs. (12)–(14) and (18) for the case of $Ri = \infty$ (pure free convection) governing the micropolar fluid flow reduce to those of Na [25] in his study of the conjugate heat transfer characteristics of Newtonian fluid flow along a vertical slender hollow circular cylinder. Furthermore, for the case of $p = 0$ (isothermal), these equations simplify to those of Chen and Mucoglu [2], who studied the mixed convection characteristics of Newtonian fluid flow. In these cases, Eq. (13) has no significance and can be omitted.

To simplify the analysis of problem, another pseudo variable ξ is introduced as following:

$$\xi = \frac{\zeta}{1+\zeta}. \tag{19}$$

Substituting the Eq. (19) into the Eqs. (12)–(14), yields

$$(1+\Delta)(1+\sigma\eta)F''' + (1+\Delta)\sigma F'' + \frac{1}{2}FF'' + \Delta G' + Ri\left(\frac{\xi}{1-\xi}\right)\theta = \xi(1-\xi)\left(F'\frac{\partial F'}{\partial \xi} - F''\frac{\partial F}{\partial \xi}\right), \tag{20}$$

$$\lambda(1+\sigma\eta)G'' + \frac{1}{2}FG' + \frac{1}{2}F'G - \frac{\Delta B}{2}\sigma^2 G - \frac{1}{4}\left(\frac{\sigma}{1+\sigma\eta}\right)FG + \frac{1}{4}\left(\frac{\sigma}{1+\sigma\eta}\right)\eta F'G - \frac{\Delta B}{4}\sigma^2(1+\sigma\eta)F'' = \xi(1-\xi)\left[\frac{1}{2}\left(\frac{\sigma}{1+\sigma\eta}\right)G\frac{\partial F}{\partial \xi} + F'\frac{\partial G}{\partial \xi} - G'\frac{\partial F}{\partial \xi}\right], \tag{21}$$

$$\frac{1}{Pr}(1+\sigma\eta)\theta'' + \frac{1}{Pr}\sigma\theta' + \frac{1}{2}F\theta' = \xi(1-\xi)\left(F'\frac{\partial \theta}{\partial \xi} - \theta'\frac{\partial F}{\partial \xi}\right). \tag{22}$$

Following transformation, the corresponding boundary conditions given in Eqs. (18a) and (18b) can be transformed to following:

At $\eta = 0$:

$$F'(\xi,0) = 0, \quad F(\xi,0) = -2\xi(1-\xi)\left.\frac{\partial F}{\partial \xi}\right|_{\eta=0},$$

$$G(\xi,0) = -\frac{1}{2}F''(\xi,0), \quad p\left(\frac{\xi}{1-\xi}\right)^{-1/2}\theta'(\xi,0) = \theta(\xi,0) - 1. \tag{23a}$$

As $\eta \to \infty$:

$$F'(\xi,\infty) = 1, \quad G(\xi,\infty) = \theta(\xi,\infty) = 0. \tag{23b}$$

In practically applications, the physical quantities of interest include the dimensionless interfacial temperature distribution, θ_w, the skin friction coefficient, C_f and the local Nusselt number, Nu_x. These quantities are derived as follows.

From the definition of the dimensionless wall temperature, it can be shown that

$$\theta_w = \theta(\xi,0) = \frac{T_w - T_\infty}{T_0 - T_\infty}. \tag{24}$$

The skin friction coefficient is defined as $C_f = 2\tau_w/\rho U_\infty^2$, and is derived from

$$C_f Re_x^{1/2} = 2\left(1 + \frac{\Delta}{2}\right)F''(\xi,0), \tag{25}$$

where $\tau_w = [(\rho\nu + \kappa)\partial u/\partial r + \kappa N]_{r=r_o}$ is the wall shear stress. Finally, from Fourier's law $q_w = -K_f\partial T/\partial r|_{r=r_o}$ and the local Nusselt number $Nu_x = q_w x/K_f(T_0 - T_\infty)$, it can be shown that the dimensionless heat transfer rate is given by

$$\frac{Nu_x}{Re_x^{1/2}} = -\theta'(\xi,0). \tag{26}$$

3. Numerical method

Due to the coupled nature of the current system, the system of non-linear equations given in Eqs. (20)–(22) and the associated boundary conditions in Eq. (23) must be solved simultaneously. The solution of the system of steady equations was obtained in previous studies using a pseudo-transient formulation approach in which a false transient term was introduced into each equation [24,28].

However, the present study solves the coupled non-linear partial differential equations using the cubic spline collocation method [28–31] together with a finite difference approximation.

Eqs. (20)–(22) using the false transient technique in discretized form are given by

$$\frac{u_{i,j}^{n+1}-u_{i,j}^{n}}{\Delta\tau}=(1+\Delta)(1+\sigma_i\eta_j)L_{u_{i,j}}^{n+1}+\left[(1+\Delta)\sigma_i+\frac{1}{2}F_{i,j}^{n}+\xi_i(1-\xi_i)\frac{F_{i,j}^{n}-F_{i-1,j}^{n}}{\Delta\xi_i}\right]l_{u_{i,j}}^{n+1}+\Delta l_{G_{i,j}}^{n}+Ri\left(\frac{\xi_i}{1-\xi_i}\right)\theta_{i,j}^{n+1}-\xi_i(1-\xi_i)u_{i,j}^{n}\frac{u_{i,j}^{n}-u_{i-1,j}^{n}}{\Delta\xi_i},\tag{27}$$

$$\frac{G_{i,j}^{n+1}-G_{i,j}^{n}}{\Delta\tau}=\lambda(1+\sigma_i\eta_j)L_{G_{i,j}}^{n+1}+\left[\frac{1}{2}F_{i,j}^{n}+\xi_i(1-\xi_i)\frac{F_{i,j}^{n}-F_{i-1,j}^{n}}{\Delta\xi_i}\right]l_{G_{i,j}}^{n+1}+\left[\frac{1}{2}u_{i,j}^{n+1}-\frac{\Delta B}{2}\sigma_i^2-\frac{1}{4}\left(\frac{\sigma_i}{1+\sigma_i\eta_j}\right)F_{i,j}^{n+1}+\frac{1}{4}\left(\frac{\sigma_i}{1+\sigma_i\eta_j}\right)\eta_j u_{i,j}^{n+1}-\frac{1}{2}\xi_i(1-\xi_i)\left(\frac{\sigma_i}{1+\sigma_i\eta_j}\right)\frac{F_{i,j}^{n}-F_{i-1,j}^{n}}{\Delta\xi_i}\right]G_{i,j}^{n}-\frac{\Delta B}{4}(1+\sigma_i\eta_j)\sigma_i^2 l_{u_{i,j}}^{n+1}-\xi_i(1-\xi_i)u_{i,j}^{n+1}\frac{G_{i,j}^{n}-G_{i-1,j}^{n}}{\Delta\xi_i},\tag{28}$$

$$\frac{\theta_{i,j}^{n+1}-\theta_{i,j}^{n}}{\Delta\tau}=\frac{1}{Pr}(1+\sigma_i\eta_j)L_{\theta_{i,j}}^{n+1}+\left[\frac{1}{Pr}\sigma_i+\xi_i(1-\xi_i)\frac{F_{i,j}^{n}-F_{i-1,j}^{n}}{\Delta\xi_i}+\frac{1}{2}F_{i,j}^{n}\right]l_{\theta_{i,j}}^{n+1}-\xi_i(1-\xi_i)u_{i,j}^{n+1}\frac{\theta_{i,j}^{n}-\theta_{i-1,j}^{n}}{\Delta\xi_i},\tag{29}$$

where

$$l_u=\frac{\partial u}{\partial\eta},\quad L_u=\frac{\partial^2 u}{\partial\eta^2},\quad l_G=\frac{\partial G}{\partial\eta},\quad L_G=\frac{\partial^2 G}{\partial\eta^2},\quad l_\theta=\frac{\partial\theta}{\partial\eta},\quad L_\theta=\frac{\partial^2\theta}{\partial\eta^2},\quad \Delta\xi_i=\xi_i-\xi_{i-1},\tag{30}$$

In Eqs. (27)–(29), $\Delta\tau=\tau^{n+1}-\tau^{n}$ represents the false time step, the subscript u denotes for $\partial F/\partial\eta$, and the superscript n denotes the iteration order.

After some rearrangement, Eqs. (27)–(29) can be expressed in the following spline approximation form:

$$\phi_{i,j}^{n+1}=Q_{i,j}+R_{i,j}l_{\phi_{i,j}}^{n+1}+S_{i,j}L_{\phi_{i,j}}^{n+1},\tag{31}$$

where ϕ represents the functions u, G, and θ. The quantities $Q_{i,j}$, $R_{i,j}$, and $S_{i,j}$, are known coefficients, which are calculated at previous time steps (Table 1).

In the present analysis, the cubic spline collocation method is used to generate an algorithm resulting in a single tridiagonal system containing either the function values at the grid points, the first derivatives, or the second derivatives only. Using the cubic spline relations described by Rubin and Khosla [29,30], Eq. (31) at the $n+1$th iteration can be written in the following tridiagonal form:

$$a_{i,j}\phi_{i,j-1}^{n+1}+b_{i,j}\phi_{i,j}^{n+1}+c_{i,j}\phi_{i,j+1}^{n+1}=d_{i,j},\tag{32}$$

where ϕ represents the function (u, G and θ) and its first and second order derivatives. Therefore, Eq. (32) is readily solved by the Thomas algorithm.

The present computational procedure commences by solving the energy equation, which provides the temperature field necessary for the solution of the reduced stream function equation. Solution of the transformed angular momentum equation for G then completes the procedure. This computation cycle is repeated until convergence is obtained. The criterion applied when assessing the convergence of the solutions is that the maximum relative change in all of the dependent variables should satisfy

$$\frac{|\phi_{i,j}^{n+1}-\phi_{i,j}^{n}|_{\max}}{|\phi_{i,j}^{n}|_{\max}}<5\times10^{-7}.\tag{33}$$

4. Results and discussion

The aim of this study was to investigate the flow and heat transfer characteristics for the forced convection of a micropolar fluid flow along a vertical slender circular hollow cylinder with wall conduction and buoyancy effects. Hence, the numerical computations were performed with $B=1\times10^5$, $\lambda=5.0$ and $Re=250$. The remaining parameters were specified as follows: micropolar parameter $\Delta=0$–12.0; Prandtl number 0.73–30.0; and Richardson

Table 1
Coefficients of Eq. (31)

ϕ	Q	R	S
u	$\Delta\tau\left[\Delta l_{G_{i,j}}^{n}+Ri\frac{\xi_i}{1-\xi_i}\theta_{i,j}^{n+1}-\xi_i(1-\xi_i)u_{i,j}^{n}\frac{u_{i,j}^{n}-u_{i-1,j}^{n}}{\Delta\xi_i}\right]+u_{i,j}^{n}$	$\Delta\tau\left[(1+\Delta)\sigma_i+\frac{1}{2}F_{i,j}^{n}+\xi_i(1-\xi_i)\frac{F_{i,j}^{n}-F_{i-1,j}^{n}}{\Delta\xi_i}\right]$	$\Delta\tau(1+\Delta)(1+\sigma_i\eta_j)$
G	$\Delta\tau\left\{\left[\frac{1}{2}u_{i,j}^{n+1}-\frac{\Delta B}{2}\sigma_i^2-\frac{1}{4}\left(\frac{\sigma_i}{1+\sigma_i\eta_j}\right)F_{i,j}^{n+1}+\frac{1}{4}\left(\frac{\sigma_i}{1+\sigma_i\eta_j}\right)\eta_j u_{i,j}^{n+1}-\frac{1}{2}\xi_i(1-\xi_i)\left(\frac{\sigma_i}{1+\sigma_i\eta_j}\right)\frac{F_{i,j}^{n}-F_{i-1,j}^{n}}{\Delta\xi_i}\right]G_{i,j}^{n}-\frac{\Delta B}{4}(1+\sigma_i\eta_j)\sigma_i^2 l_{u_{i,j}}^{n+1}-\xi_i(1-\xi_i)u_{i,j}^{n+1}\frac{G_{i,j}^{n}-G_{i-1,j}^{n}}{\Delta\xi_i}\right\}+G_{i,j}^{n}$	$\Delta\tau\left[\frac{1}{2}F_{i,j}^{n}+\xi_i(1-\xi_i)\frac{F_{i,j}^{n}-F_{i-1,j}^{n}}{\Delta\xi_i}\right]$	$\Delta\tau\lambda(1+\sigma_i\eta_j)$
θ	$\Delta\tau\xi_i(1-\xi_i)u_{i,j}^{n+1}\frac{\theta_{i,j}^{n}-\theta_{i-1,j}^{n}}{\Delta\xi_i}+\theta_{i,j}^{n}$	$\Delta\tau\left[\frac{1}{Pr}\sigma_i+\frac{1}{2}F_{i,j}^{n}+\xi_i(1-\xi_i)\frac{F_{i,j}^{n}-F_{i-1,j}^{n}}{\Delta\xi_i}\right]$	$\frac{\Delta\tau}{Pr}(1+\sigma_i\eta_j)$

number $Ri = 0.0$–20.0. The conjugate heat transfer parameter, p, is ranged 0.0–0.75 to conform to the practical cases. For example, the fluid (for water: $K_f = 0.628$ W/m K) flows along a slender stainless steel tubes with $r_o = 0.03$ m, $r_i = 0.02$ m and $K_s = 15$ W/m K, we can find the conjugate heat transfer parameter $p = 0.27$.

To assess the accuracy of the cubic spline collocation method, the present numerical results were compared with the published data [2] resulting to the mixed convection of a Newtonian fluid flow along a vertical isothermal ($p = 0.0$) cylinder with $\Delta = B = \lambda = 0$, and $Pr = 0.7$. For different values of ξ, the current results for the dimensionless liquid–solid interfacial heat transfer rate, $-\theta(\xi,0)$, and the skin friction factor, $f''(\xi,0)$, are in a good agreement with those of [2], as shown in Table 2.

The variation of the dimensionless interfacial temperature distributions as a function of ξ in the boundary layer of the micropolar fluid are shown in Fig. 2 for four different values of p with $Pr = 10.0$, $\Delta = 1.0$ and $Ri = 2.0$. The solution of the isothermal case ($p = 0$), the wall temperature is uniform at T_0 ($\theta_w = 1$), is represented by a horizontal straight line. It can be seen that the temperature of the fluid on the wall increases monotonically with ξ for a given value of p. Comparing with isothermal cylinder ($p = 0$), an increase in the conjugate heat transfer parameter, p, causes a reduction in the interfacial temperature. This is because an increased value of p corresponds to a lower wall conductance K_s and promote a greater surface temperature variations.

Fig. 3 plots the variation of the dimensionless interfacial temperature profiles as a function of ξ, for selected values of Δ. As in the case above, the dimensionless interfacial temperature increases with increasing ξ. Furthermore, it is observed that the dimensionless interfacial temperature is higher for micropolar fluids than for Newtonian fluids (the limiting case of $\Delta = 0$). In addition, the higher the value of Δ, the greater the dimensionless interfacial temperature.

Fig. 4 presents the variation of the interfacial temperature with ξ for various values of the Ri. It can be seen that as the value of ξ increases, the interfacial temperature rises, i.e. the interfacial temperature increases from the bottom of the cylinder towards the top of the cylinder. Compared with the limiting case of $Ri = 0$ (i.e. pure forced convection), an increase in the value of Ri gives rise to a reduced interfacial temperature since a greater value of Ri indicates a greater buoyancy effect, which increases the convection cooling effect and hence reduces the wall temperature.

Table 2
Comparison of the local wall heat transfer rate with $Pr = 0.7$, $Ri = 0$, $p = 0.0$ (isothermal) and $\Delta = B = \lambda = 0$ (Newtonian fluid)

$\frac{4}{r_o}\left(\frac{vx}{U_\infty}\right)^{1/2}$	Chen and Mucoglu [2]		Present results	
	$f''(\xi,0)$	$-\theta(\xi,0)$	$f''(\xi,0)$	$-\theta(\xi,0)$
0.0	1.3282	0.5854	1.3280	0.5852
1.0	1.9172	0.8669	1.9133	0.8658
2.0	2.3981	1.0968	2.3900	1.0940
3.0	2.8270	1.3021	2.8159	1.2998
4.0	3.2235	1.4921	3.2187	1.4925

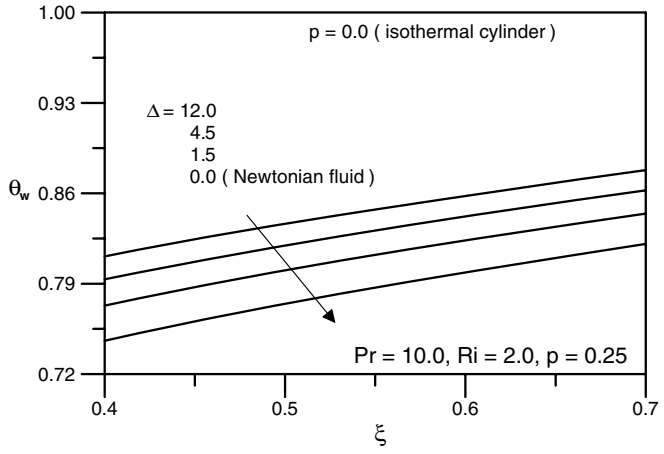

Fig. 3. Variation of interfacial temperature with ξ at different values of Δ.

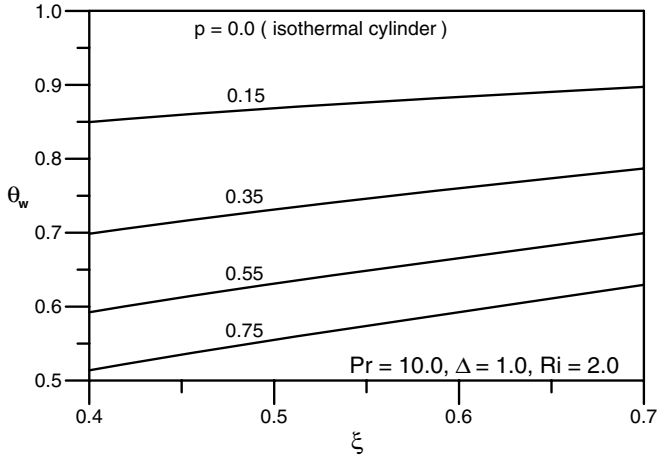

Fig. 2. Variation of interfacial temperature with ξ at different values of p.

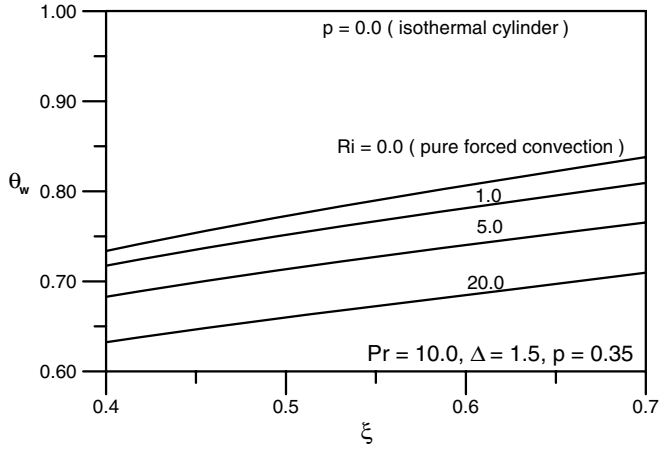

Fig. 4. Variation of interfacial temperature with ξ at different values of Ri.

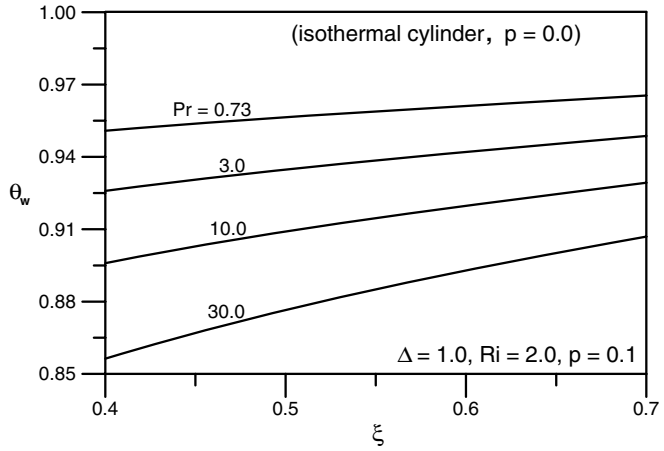

Fig. 5. Variation of interfacial temperature with ξ at different values of Pr.

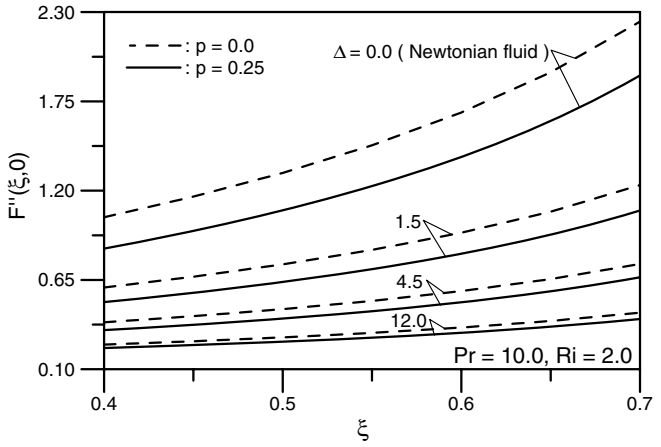

Fig. 7. Effect of micropolar material parameter Δ on skin friction factor.

Fig. 5 presents the variation of the interfacial temperature with ξ for various values of the Prandtl number, Pr. The results indicate that an increase in the value of Pr give rise to a reduced interfacial temperature since a greater value of Pr indicates a higher heat transfer coefficients.

It is shown on Fig. 6 to indicate the influence of the conjugate heat transfer parameter, p, on the skin friction factor. The dashed lines and solid lines in the figure indicate the skin friction factor corresponding to the cases of isothermal cylinder ($p = 0$) and non-isothermal cylinder ($p > 0$), respectively. It can be seen that the local skin friction factor decreases with an increasing value of p and increases along the streamwise direction. This is because the increasing interfacial temperature along the streamwise direction generates greater buoyancy effects, and hence increases the skin friction factor.

Fig. 7 illustrates the effect of the micropolar material parameter, Δ, on the skin friction factor for $Pr = 10.0$ and $p = 0.0$ (dashed lines) and $p = 0.25$ (solid lines), respectively. It shows that the skin friction factor is lower for micropolar fluids than for Newtonian fluids ($\Delta = 0$) since micropolar fluids offer a greater resistance to the fluid motion compared to Newtonian fluid. The results also indicate that the larger the value of Δ, the lower the skin friction factor. Moreover, while the greater values of micropolar material parameter, Δ, the less sensitivity of the wall conduction effects influence to the skin friction factor.

Fig. 8 illustrates the effect of the buoyancy force on the skin friction factor for $Pr = 10.0$, $\Delta = 1.5$ and $p = 0$ (dashed lines) and 0.35 (solid lines), respectively. It is observed that the local skin friction factor increases as the buoyancy effect increases. The reason for this is that an increase in the buoyancy effect in mixed convection flow leads to an acceleration of the fluid flow, which increases the local skin friction factor. Additionally, the higher the value of the buoyancy effect, the more the sensitivity of the wall conduction effects influences the skin friction factor. In the limiting case of $Ri = 0$, i.e. pure forced convection with no buoyancy effects, the conjugate heat transfer parameter, p, is virtually independent of the skin friction factor because the buoyancy effect generated by the temperature difference is relatively weaker.

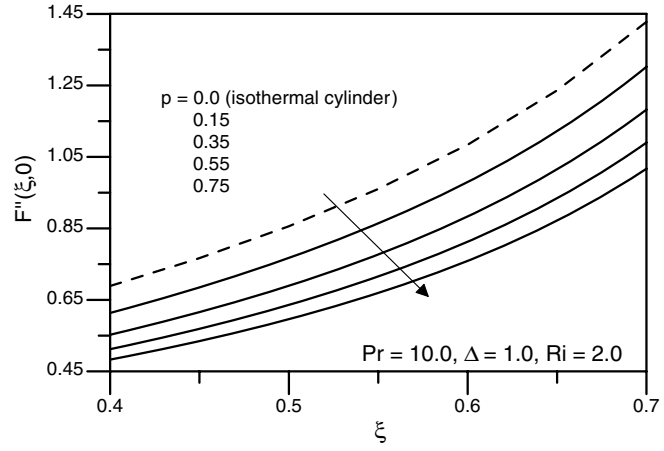

Fig. 6. Effect of conjugate heat transfer parameter p on skin friction factor.

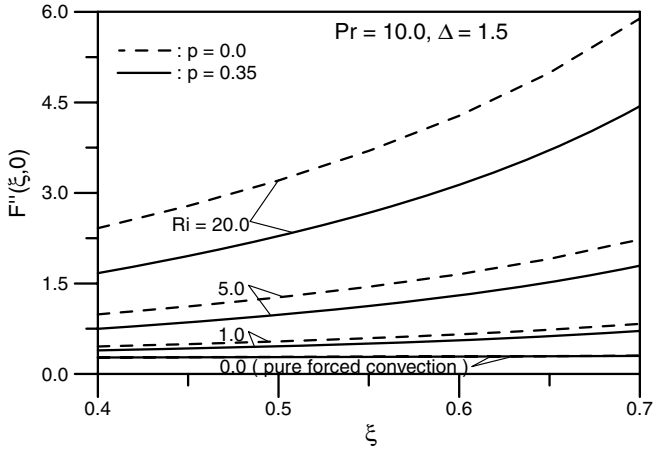

Fig. 8. Effect of Richardson number Ri on skin friction factor.

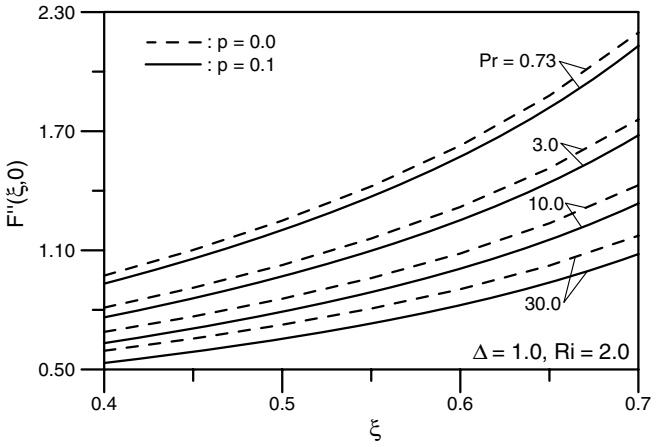

Fig. 9. Effect of Prandtl number *Pr* on skin friction factor.

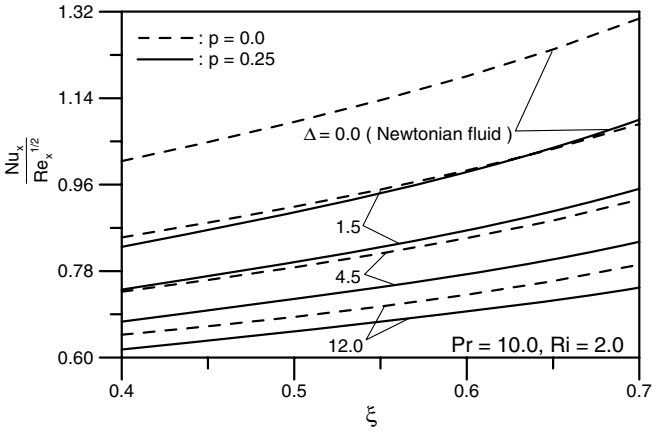

Fig. 11. Effect of micropolar material parameter Δ on heat transfer rate.

Fig. 9 plots the variation of the skin friction factor along the streamwise direction for various values of Prandtl number, *Pr*. Note that the dashed line corresponds to the case of an isothermal cylinder ($p = 0$). It reveals that the local skin friction factor decreases as *Pr* increases. Because of an increase in *Pr* means the greater density of fluids, and hence causes a reduction in the buoyancy effect.

Fig. 10 shows the effect of the conjugate heat transfer parameter, *p*, on the local heat transfer rate along the streamwise direction, ξ. As in the case above, the dashed line corresponds to an isothermal cylinder ($p = 0$). It can be seen that the local heat transfer rate increases as ξ increases. Furthermore, the effect of conjugate heat transfer gives rise to a reduction of the local heat transfer rate, i.e. the greater the value of *p*, the lower the local heat transfer rate. This trend is consistent with the interfacial temperature distributions presented in Fig. 2.

Fig. 11 plots the local heat transfer rate for different values of the micropolar material parameter, Δ. The results reveal that the local heat transfer rate decreases as the value of Δ increases. This trend is not only occurring on isothermal cylinder ($p = 0$, the dashed line), but also on the non-isothermal cylinder ($p > 0$, the solid lines). This is due to that greater Δ increases the thickness of thermal boundary layer which results in lower the local heat transfer rate. Furthermore, the higher values of micropolar material parameter Δ means that the greater resistance in fluid, thereby leads to the higher wall temperature and decreases the influence of conjugate heat transfer parameter *p*.

Fig. 12 illustrates the effect of the buoyancy force on the local heat transfer rate. It is noted that as the value of the *Ri* increases, the local heat transfer rate also increases, both for the case of an isothermal cylinder (dashed lines) and a non-isothermal cylinder (solid lines). This is because an increased buoyancy effect generates a greater buoyancy force, which increases the fluid velocity, and hence raises the local heat transfer rate. The effect of the conjugate heat transfer parameter, *p*, is more significant at higher values of *Ri*, but is less pronounced for pure forced convection ($Ri = 0$).

Fig. 13 illustrates the variations of the local heat transfer rate with ξ for different values of the Prandtl number, *Pr*. As in the case above, the dashed lines indicate an isothermal cylinder ($p = 0$), while the solid lines represent a non-

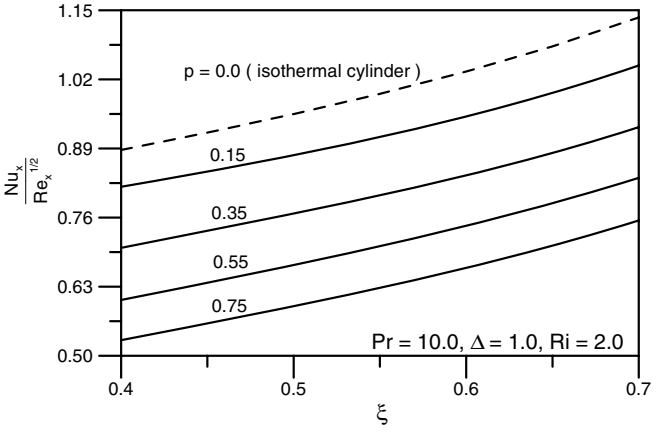

Fig. 10. Effect of conjugate heat transfer parameter *p* on heat transfer rate.

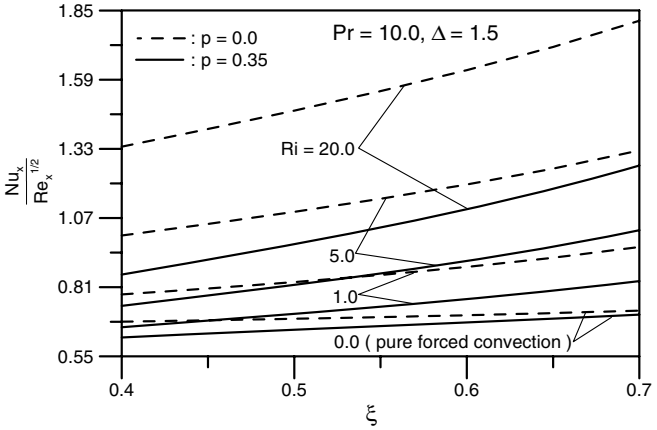

Fig. 12. Effect of Richardson number *Ri* on heat transfer rate.

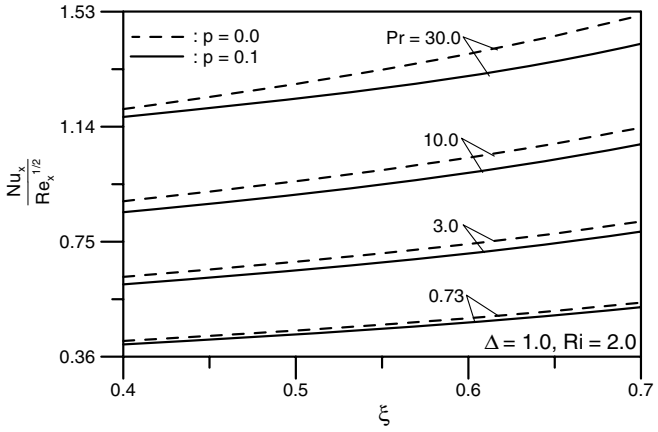

Fig. 13. Effect of Prandtl number *Pr* on heat transfer rate.

isothermal cylinder. It is observed that higher values of the Prandtl number, *Pr*, result in higher local heat transfer rate. This is because a higher Prandtl number give rise to a greater heat transfer effect, which in this case, implies a larger heat transfer rate on the wall. In addition, the effect of wall conduction on the heat transfer rate is more pronounced when *Pr* is larger.

5. Conclusions

This study has analyzed the effect of buoyancy and wall conduction on the forced convection flow of a micropolar fluid. The non-linear formulation governing equations and their associated boundary conditions have been obtained and solved using the non-similarity transform and the cubic spline collocation method, respectively. The influences of the conjugate heat transfer parameter, the Richardson number, the micropolar material parameter, and the Prandtl number on the solid–liquid interfacial temperature distribution, the skin friction factor, and the local heat transfer rate have been systematically examined. The conjugate heat transfer parameter, p, and the Richardson number, *Ri*, are identified which are the measure of the effect of wall conduction and buoyancy, respectively.

Numerical results show that the conjugate heat transfer parameter has a significant influence on the fluid flow and heat transfer characteristics. An increase in the conjugate heat transfer parameter (i.e. a stronger wall conduction effect) results in a reduction in the solid–liquid interfacial temperature distribution, the skin friction factor, and the local heat transfer rate. The effects of the wall conduction on the thermal and the flow fields are found to be more pronounced in a system with a greater Prandtl number or lager buoyancy parameter (i.e. a stronger buoyancy effect). Furthermore, the skin friction parameter, the local heat transfer rate, and the interfacial temperature all increase with increasing streamwise coordinate, ξ.

An increase in the buoyancy effect reduces the temperature distribution and increases the skin friction factor and the local heat transfer rate on the wall. The effects of the buoyancy force on the thermal and the flow fields are found to increase the effect of wall conduction. Compared to the case of pure forced convection, mixed convection (i.e. a stronger buoyancy effect) is found to result in a lower interfacial temperature but higher the local heat transfer rate and the skin friction factor.

Finally, the higher values of micropolar material parameter result in lower the skin friction parameter and higher the interfacial temperature and the local heat transfer rate. The effects of the micropolar material parameter on the thermal and the flow fields are found to decrease the effect of wall conduction. The effect of conjugate heat transfer parameter, p, on the characteristics of the thermal and the flow fields is less sensitive in a system with a greater micropolar material parameter.

References

[1] J.R. Lloyd, M. Sparrow, Combined force and free convection flow on vertical surfaces, Int. J. Heat Mass Transfer 13 (1970) 434–438.
[2] T.S. Chen, A. Mucoglu, Buoyancy effects on forced convection along a vertical cylinder, ASME J. Heat Transfer 97 (1975) 198–203.
[3] A. Mucoglu, T.S. Chen, Buoyancy effects on forced convection along a vertical cylinder with uniform surface heat flux, ASME J. Heat Transfer 98 (1976) 523–525.
[4] I.G. Choi, The effect of variable properties of air on the boundary layer for a moving continuous cylinder, Int. J. Heat Mass Transfer 25 (1982) 597–602.
[5] S.L. Lee, T.S. Chen, B.F. Armaly, Mixed convection along vertical cylinders and needles with uniform surface heat flux, ASME J. Heat Transfer 109 (1987) 711–716.
[6] A.T. Eswara, G. Nath, Unsteady forced convection laminar boundary layer flow over a moving longitudinal cylinder, Acta Mech. 93 (1992) 13–28.
[7] T.Y. Na, I. Pop, Flow and heat transfer over a longitudinal circular cylinder moving in parallel or reversely to a free stream, Acta Mech. 118 (1996) 185–195.
[8] W. Lin, S.W. Armfield, Direct simulation of natural convection cooling in a vertical circular cylinder, Int. J. Heat Mass Transfer 42 (1999) 4117–4130.
[9] M. Kumari, G. Nath, Mixed convection boundary layer flow over a thin vertical cylinder with localized injection/suction and cooling/heating, Int. J. Heat Mass Transfer 47 (2004) 969–976.
[10] A.C. Eringen, Simple microfluids, Int. J. Eng. Sci. 2 (1964) 205–217.
[11] A.C. Eringen, Theory of thermomicrofluids, J. Mathematical Anal. Appl. 38 (1972) 480–496.
[12] T. Ariman, M.A. Turk, N.D. Sylvester, Microcontinuum fluid mechanics—a review, Int. J. Eng. Sci. 11 (1973) 905–930.
[13] G. Ahmadi, Self-similar solution of incompressible micropolar boundary layer flow over a semi-infinite plate, Int. J. Eng. Sci. 14 (1976) 639–646.
[14] S.K. Jena, M.N. Mathur, Mixed convection flow of a micropolar fluid from an isothermal vertical plate, Comput. Math. Appl. 10 (1984) 291–304.
[15] R.S.R. Gorla, A. Ameri, Boundary layer flow of a micropolar fluid on a continuous moving cylinder, Acta Mech. 57 (1985) 203–214.
[16] R.S.R. Gorla, P.P. Lin, A.J. Yang, Asymptotic boundary layer solutions for mixed convection from a vertical surface in a micropolar fluid, Int. J. Eng. Sci. 28 (1990) 525–533.
[17] A.A. Mohammadien, M. Modather, A. Salem, R.S.R. Gorla, Mixed convection flow of a micropolar fluid on a moving heated horizontal plate, J. Appl. Math. Mech. (ZAMM) 81 (2001) 549–557.
[18] P.G. Siddheshwar, C.V. Sri Krishna, Linear and non-linear analyses of convection in a micropolar fluid occupying a porous medium, Int. J. Non-linear Mech. 38 (2003) 1561–1579.

[19] R. Bhargava, L. Kumar, H.S. Takhar, Mixed convection from a continuous surface in a parallel moving stream of a micropolar fluid, Heat Mass Transfer 39 (2003) 407–413.
[20] M. Miyamoto, J. Sumikawa, T. Akiyoshi, T. Nakamura, Effect of axial heat conduction in a vertical flat plate on free convection heat transfer, Int. J. Heat Mass Transfer 23 (1980) 1545–1553.
[21] E.M. Sparrow, M.K. Chyu, Conjugated forced convection–conduction analysis of heat transfer in a plate fin, ASME J. Heat Transfer 104 (1982) 204–206.
[22] J. Timma, J.P. Padet, Etude théorique du couplage convection–conduction en convection libre laminaire sur une plaque verticale, Int. J. Heat Mass Transfer 28 (1985) 1097–1104.
[23] A. Pozzi, M. Lupo, The coupling of conduction with laminar natural convection along a flat plate, Int. J. Heat Mass Transfer 31 (1988) 1807–1814.
[24] M.I. Char, C.K. Chen, J.W. Cleaver, Conjugate forced convection heat transfer from a continuous, moving flat sheet, Int. J. Heat Fluid Flow 11 (1990) 257–261.
[25] T.Y. Na, Effect of wall conduction on natural convection over a vertical slender hollow circular cylinder, Appl. Sci. Res. 54 (1995) 39–50.
[26] A.Z. Vaszi, D.B. Ingham, D. Lesnic, D. Munslow, I. Pop, Conjugate free convection from a slightly inclined plate embedded in a porous medium, J. Appl. Math. Mech. (ZAMM) 81 (2001) 465–479.
[27] G. Jilani, S. Jayaraj, M.A. Ahmad, Conjugate forced convection–conduction heat transfer analysis of a heat generating vertical cylinder, Int. J. Heat Mass Transfer 45 (2002) 331–341.
[28] G.S. Rubin, R.A. Graves, Viscous flow solution with a cubic spline approximation, Comput. Fluids 3 (1975) 1–36.
[29] G.S. Rubin, P.K. Khosla, Higher-order numerical solutions using cubic splines, AIAA J. 14 (1976) 851–858.
[30] G.S. Rubin, P.K. Khosla, Polynomial interpolation methods for viscous flow calculation, J. Comput. Phys. 24 (1977) 217–244.
[31] P. Wang, R. Kahawita, Numerical integration of partial differential equations using cubic splines, Int. J. Comput. Math. 13 (1983) 271–286.